Viscoelastic Properties of the Rat Brain in the Horizontal Plane.

John D. Finan[1], Erica M. Pearson[1], Barclay Morrison III[1]

Abstract Traumatic brain injury (TBI) is a widespread, devastating and difficult to treat medical condition initiated by complex biomechanical mechanisms. Rodent models of TBI are widely used to study the pathobiology, but data needed to fully characterize the mechanics of these injury models is lacking. In this study, the viscoelastic properties of specific regions of the rat brain were measured by microindentation of slices prepared in the horizontal anatomical plane. These data complement previously reported data acquired in the sagittal and coronal plane to provide insight into the anisotropy of region-specific properties of the rat brain. As in the sagittal and coronal planes, brain properties in the horizontal plane were age, time and region dependent. There was evidence of anisotropy in the alveus and corpus callosum. These data will support the next generation of computational models of TBI that will yield greater understanding of its biomechanics.

Keywords Anisotropy, brain, properties, rat, viscoelastic.

I. INTRODUCTION

Traumatic brain injury is a devastating societal problem that causes approximately 50,000 deaths along with $76.5 billion in direct and indirect costs in the United States each year[1]. The progression of brain injury after a traumatic event involves a complex array of pathological processes[2]. Rat models of TBI are commonly used to study these processes[3]. One source of variation leading to pathological complexity is the heterogeneity of the brain itself. The consequences of brain damage may depend on the structures involved because distinct anatomical structures each have a different function. Rat models enable biological investigation of the effect of structural heterogeneity on TBI. However, to relate these biological findings to mechanical loading, a mechanical model that explicitly accounts for the different mechanical properties of different anatomical structures is required.

Finite element modeling can predict the loading of various anatomical structures during a traumatic event[4]. However, there are several challenges involved in creating a model that is sufficiently detailed and accurate to generate useful predictions. A refined and anatomically accurate mesh is necessary to capture the irregular geometry of the rat brain. This geometric information is now accessible from high resolution MRI or CT scans, and the resulting high degree of freedom models can typically be solved in a reasonable time frame with modern computing resources. A tolerance criterion is also necessary to relate tissue strain to loss of function[5]. Finally, accurate mechanical properties for the different anatomical regions of the brain are needed to populate the model.

Brain tissue is a complex, non-linear material, particularly in the strain and strain rate domain associated with TBI (strain > 10% and strain rate > 10 s^{-1} [6]). The mechanical properties of brain have been found to be viscoelastic [7-9], non-linear [10], age dependent [8, 11, 12] and anisotropic [13]. In addition, experimental factors during testing significantly influence results and so must be carefully controlled. The mechanical properties reported in the literature vary widely [14] and much of this variation is attributed to differences in time postmortem, tissue fixation or tissue preparation [15]. To minimize the effect of postmortem degradation of the tissue, we imposed a strict time-limit on the interval between animal sacrifice and conclusion of data collection. The tissue was not fixed or preconditioned so that the results would mimic the *in situ* response as closely as possible. An indentation loading mode was selected so that the local properties of several different anatomical regions could be tested in rapid succession [16]. This mode of loading also minimizes the amount of

J. D. Finan is a post-doctoral research scientist in the Department of Biomedical Engineering at Columbia University in New York. E. M. Pearson is an undergraduate research assistant in the Department of Biomedical Engineering at Columbia University in New York. B. Morrison III is a Professor in the Department of Biomedical Engineering at Columbia University in New York (phone: +1 212-854-6277, fax: +1 212-854-8725, email: bm2119@columbia.edu).

glue needed experimentally because the load was not transmitted to the tissue via an adhesive bond. The goal of this study in the horizontal plane was to complement earlier studies of the mechanical properties of the rat brain which employed indentation in the coronal [17] and sagittal [18] planes and to support the development of predictive computational models of TBI in the rat.

II. METHODS

Sample Preparation

Adult (250 – 350g) and juvenile (P17/18) rats were sacrificed via CO_2 inhalation and the brains were immediately removed, blocked and cut into slices using a vibratome (Vibratome 1000 plus, The Vibratome Company) or a tissue chopper (McIlwain tissue chopper, The Mickle Laboratory Engineering Co. Ltd.). The slices were 1mm thick for hind brain regions (cerebellum grey matter, cerebellum white matter and brain stem) and 2mm thick for forebrain regions (cortex, alveus, thalamus, hippocampus CA1, hippocampus CA3 and dentate gyrus). These slices were adhered to the bottom of a Petri dish and submerged in CO_2-independent medium (Invitrogen) for testing. The regions tested are described in Figure 1. The cortex was subdivided into three regions in the adult (inner, middle and outer) while it was treated as a single region in the juvenile animal because of its reduced sized.

Indentation

The Petri dish containing the sample was mounted on a 10g load cell (GSO-10, Transducer Techniques) that was in turn placed on a motorized microscope stage and positioned beneath the indenter device. The indenter device consisted of a 500 µm diameter flat ended cylindrical punch (National Jet Company) mounted on a linear actuator (M-227.10, Physik Instrumente) and monitored by a displacement sensor (capaNCDT 6100, Micro-Epsilon). Load and displacement data were collected at 10 kHz via a custom LabView (National Instruments) program that also controlled the linear actuator. The tip of the indenter was incrementally brought to the surface of the tissue until a tare load of 1-2 mg was established. Then, a step indentation to a depth of 39.3 µm was applied in a period of approximately 70 ms and sustained for 20 seconds. This depth was chosen to create an equivalent strain of 10% under the indenter tip according to the formula for averaging the spatially inhomogeneous strain field due to indentation that was previously presented [17]. After testing, the indenter was slowly withdrawn and the motorized stage was repositioned to allow testing of another region. The sequence in which the various regions were tested was randomized before each experiment and all testing was completed within 2 hours of animal sacrifice.

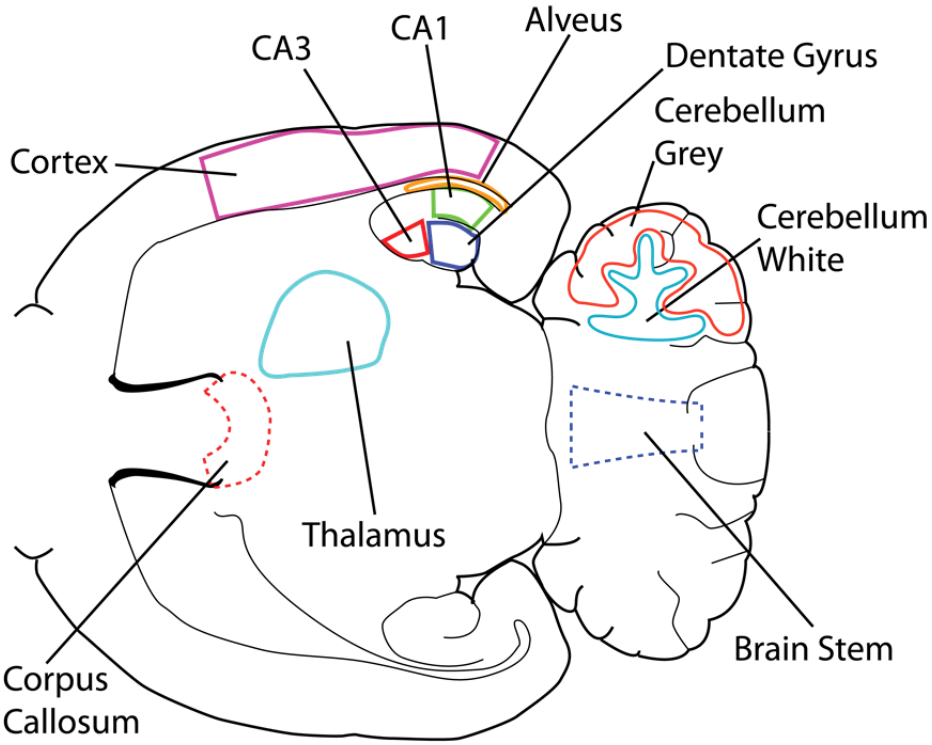

Figure 1: Definition of anatomical regions for the purposes of indentation. Dashed lines denote regions that were defined at the location shown but at a lower horizontal section than the one shown in this image.

Mathematical Model

The mathematical treatment was identical to that used previously [18]. Briefly, the model described indentation of a viscoelastic layer of infinite horizontal extent but finite vertical thickness. The material was assumed to be isotropic and incompressible and strains were assumed to be small. The solution for elastic indentation of an infinite half-space was given by Sneddon [19] as follows:

$$P = \frac{4R\delta G}{1-\nu} \quad (1)$$

where P is the indentation load, R is the indenter radius, δ is the indentation depth, G is the shear modulus and ν is the Poisson's ratio. Hayes modified this expression to incorporate the effect of finite sample thickness [20] as follows:

$$P = \frac{4\kappa R\delta G}{1-\nu} \quad (2)$$

The factor κ has a value greater than one that increases as the ratio of indenter radius to layer thickness increases because an increasing fraction of the applied load is transmitted to the rigid substrate via compression of the material beneath the indenter. The value of κ in this study was 1.37 and 1.16 for tissue slices that were 1mm and 2mm thick respectively. Viscoelastic effects were introduced using the hereditary integral approach of Lee and Radok [21] to explicitly describe the displacement history as follows:

$$P(t) = \frac{4R\kappa}{1-\nu}\int_0^t G(t-\tau)\left(\frac{d\delta}{d\tau}\right)d\tau \quad (3)$$

Explicit description of the displacement history eliminates the need to approximate the displacement history as a step and thereby allows us to determine mechanical properties relating to times before the end of the ramp. The following Prony series expression was used to describe the relaxation function, G(t).

$$G(t) = G_\infty + \sum_j G_j e^{-\frac{t}{\tau_j}} \quad (4)$$

where G_∞ is the equilibrium modulus, G_j is a coefficient, t is time and τ_j is a time constant. The number of terms, j, was determined dynamically using the F-statistic to determine if the improvement in the fit associated with the addition of a further term was statistically significant [22]. The values of the coefficients of the Prony series were determined by numerical fitting of expression (3) to the experimentally acquired load history in Matlab (Mathworks). An individual relaxation function was computed for each test.

Statistics

Time-dependent moduli values were computed for the purposes of preparing descriptive and comparative statistics. Three time points were chosen: 10 ms, 50 ms and 20 seconds. These time points were chosen because the first two represent reasonable estimates for the upper and lower bounds of the time domain on which impact trauma occurs while the last represents the closest approximation to infinite time (i.e. equilibrium) in our data set. The value of G(t) was computed at each of these time points for each test using the relaxation function fit to that test. These values were compared to test for the effect of animal age, anatomical region and time using a three-way ANOVA. Subsequent *post-hoc* tests for statistically significant differences between different regions at the 10 ms time point were conducted using a Bonferroni correction. A regional relaxation function was determined for each region by fitting expression (3) to the average load history for that region. The statistical significance of the difference between the relaxation functions for the different regions was determined using a Kolmogorov Smirnov statistic with 50 log-distributed comparison points and Bonferroni correction [23].

III. RESULTS

The average time dependent moduli are reported in Figure 2 and Figure 3 for adult and juvenile brain, respectively. An ANOVA revealed significant ($p < 0.05$) main effects of anatomical region, time and age, indicating that the tissue is spatially heterogeneous, viscoelastic and that its properties change as the animal matures. In the adult animal, the hind brain regions tested were softer than the forebrain regions tested. In the juvenile animal, the cerebellum was softer than the other regions tested. Figure 4 shows the regional relaxation functions for the adult while Figure 5 shows the regional relaxation functions for the juvenile. The coefficients for these relaxation functions are tabulated in Table 1 and Table 2, respectively. The relaxation function was optimally represented by a three term Prony series in all but 2 of the 22 scenarios presented. Typically, the first time constant was on the order of tens of milliseconds, the second was on the order of hundreds of milliseconds and the last was on the order of seconds. The 95% confidence intervals for the time constants are typically 50% of the mean or less while the 95% confidence intervals for the moduli are typically 25% of the mean or less.

(a)

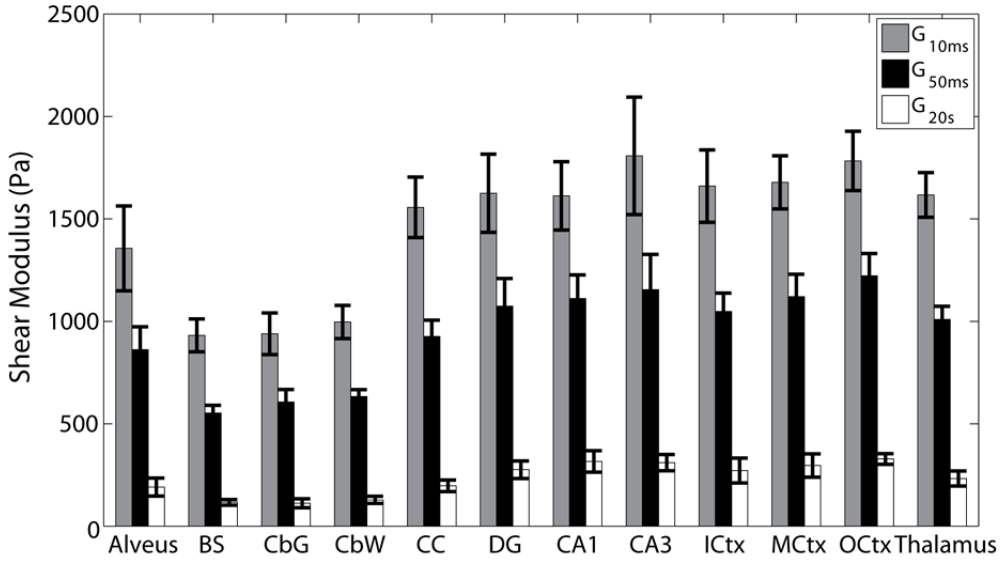

(b)

	Alveus	BS	CbG	CbW	CC	DG	CA1	CA3	ICtx	MCtx	OCtx
BS	-										
CbG	-	-									
CbW	-	-	-								
CC	-	-	-	-							
DG	-	-	-	-	-						
CA1	-	-	-	-	-	-					
CA3	-	*	*	*	-	-	-				
ICtx	-	o	o	-	-	-	-	-			
MCtx	-	o	o	-	-	-	-	-	-		
OCtx	-	*	*	o	-	-	-	-	-	-	
Thalamus	-	-	-	-	-	-	-	-	-	-	-

Figure 2: (a) Time-dependent shear moduli for adult rat brain tissue by region (error bars = standard error, $n \geq 5$). (b) *Post-hoc* Bonferroni comparisons between regions for time-dependent shear modulus value at 10 ms (- = $p > 0.1$, o = $p \leq 0.1$, * = $p \leq 0.05$). BS = brain stem, CbG = cerebellum grey matter, CbW = cerebellum white matter, CC = corpus callosum, DG = dentate gyrus, CA1 = hippocampus CA1, CA3 = hippocampus CA3, ICtx = inner cortex, MCtx = middle cortex, OCtx = outer cortex.

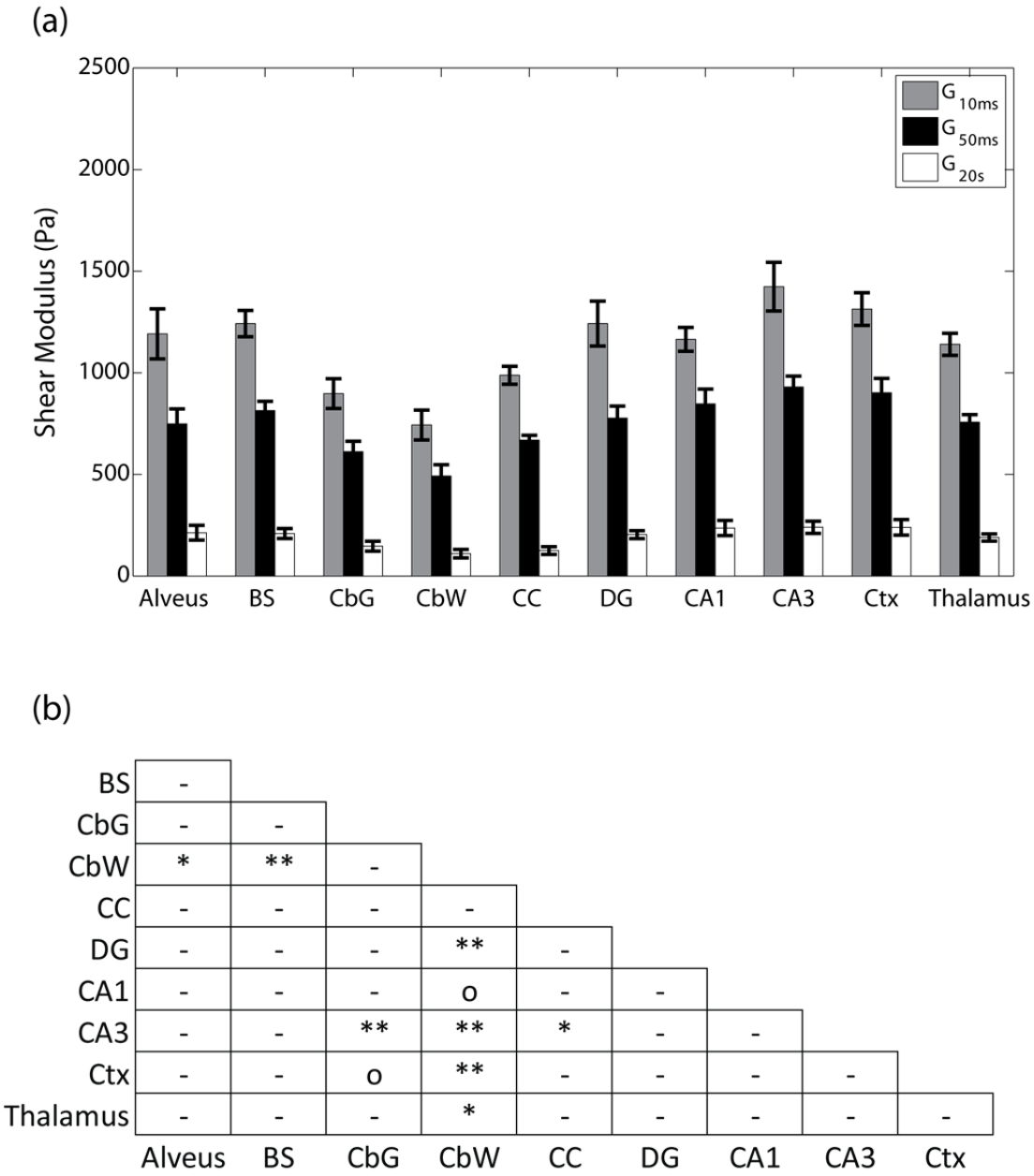

Figure 3: (a) Time-dependent shear moduli for the juvenile (P17/18) rat brain by region (error bars = standard error, n ≥ 6). (b) *Post-hoc* Bonferroni comparisons between regions for time-dependent shear modulus value at 10 ms (- = $p > 0.1$, o = $p \leq 0.1$, * = $p \leq 0.05$, ** = $p \leq 0.01$). BS = brain stem, CbG = cerebellum grey matter, CbW = cerebellum white matter, CC = corpus callosum, DG = dentate gyrus, CA1 = hippocampus CA1, CA3 = hippocampus CA3, Ctx = cortex.

(a)

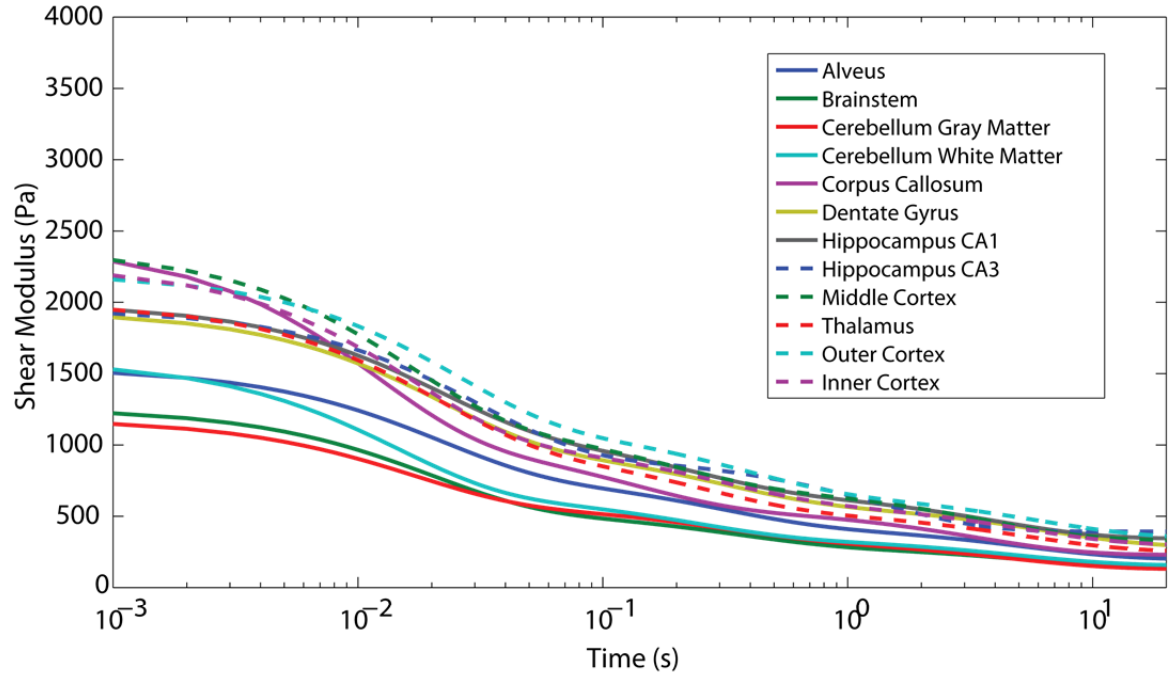

(b)

	Alveus	BS	CbG	CbW	CC	DG	CA1	CA3	ICtx	MCtx	OCtx
BS	*										
CbG	*	-									
CbW	-	*	*								
CC	*	*	*	*							
DG	*	*	*	*	*						
CA1	*	*	*	*	*	-					
CA3	*	*	*	*	*	-	-				
ICtx	*	*	*	*	-	*	*	*			
MCtx	*	*	*	*	-	*	*	*	-		
OCtx	*	*	*	*	-	*	*	*	-	-	
Thalamus	*	*	*	*	*	-	-	-	*	*	*

Figure 4: (a) Stress relaxation functions for various regions of adult rat brain. (b) Kolmogorov-Smirnov testing of statistical significance of the difference between relaxation functions for different regions (* = $p \leq 0.05$, - = $p > 0.05$).

(a)

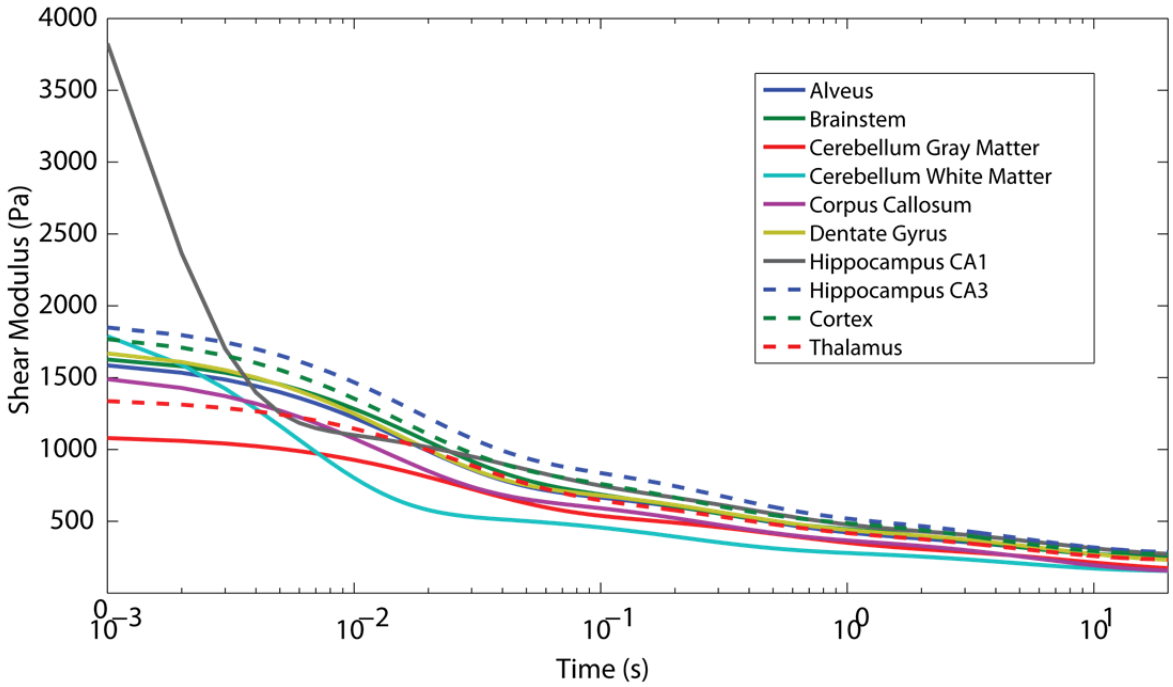

(b)

	Alveus	BS	CbG	CbW	CC	DG	CA1	CA3	Ctx
BS	-								
CbG	*	*							
CbW	-	-	*						
CC	-	*	*	*					
DG	-	-	*	-	*				
CA1	*	*	*	*	*	*			
CA3	*	*	*	-	*	*	*		
Ctx	*	*	*	-	*	-	*	-	
Thalamus	*	*	*	*	*	*	*	*	*

Figure 5: (a) Stress relaxation functions for various regions of juvenile rat brain. (b) Kolmogorov-Smirnov testing of statistical significance of the difference between relaxation functions for different regions (* = $p \leq 0.05$, - = $p > 0.05$).

TABLE 1
Coefficients of stress relaxation functions for various regions of the adult rat brain (± 95% confidence intervals).

	G_∞ (Pa)	G_1 (Pa)	τ_1 (s)	G_2 (Pa)	τ_2 (s)	G_3 (Pa)	τ_3 (s)	R^2
Alveus	198 ± 32	741 ± 115	0.0204 ± 0.0058	359 ± 59	0.284 ± 0.136	244 ± 44	5.25 ± 2.70	0.980
Brainstem	137 ± 13	709 ± 51	0.0194 ± 0.0023	249 ± 23	0.320 ± 0.088	164 ± 20	5.23 ± 1.71	0.992
Cerebellum Gray Matter	129 ± 13	594 ± 81	0.0163 ± 0.0034	246 ± 29	0.290 ± 0.100	215 ± 27	4.40 ± 1.25	0.989
Cerebellum White Matter	155 ± 12	934 ± 86	0.0141 ± 0.0019	308 ± 25	0.227 ± 0.052	198 ± 18	4.86 ± 1.20	0.991
Corpus Callosum	229 ± 12	1354 ± 180	0.0113 ± 0.0026	493 ± 60	0.128 ± 0.029	330 ± 25	3.37 ± 0.59	0.995
Dentate Gyrus	285 ± 43	931 ± 117	0.0209 ± 0.0048	411 ± 59	0.291 ± 0.121	314 ± 42	6.41 ± 2.93	0.991
Hippocampus CA1	344 ± 23	869 ± 125	0.0198 ± 0.0058	440 ± 78	0.217 ± 0.097	340 ± 49	3.97 ± 1.26	0.991
Hippocampus CA3	393 ± 13	1028 ± 71	0.0306 ± 0.0040	534 ± 28	1.350 ± 0.190			0.990
Inner Cortex	297 ± 22	1222 ± 117	0.0163 ± 0.0024	425 ± 40	0.279 ± 0.078	320 ± 33	5.10 ± 1.42	0.986
Middle Cortex	332 ± 18	1196 ± 154	0.0154 ± 0.0037	464 ± 72	0.178 ± 0.065	382 ± 40	3.65 ± 0.85	0.992
Outer Cortex	349 ± 35	1051 ± 84	0.0241 ± 0.0038	477 ± 51	0.354 ± 0.109	328 ± 40	6.02 ± 2.29	0.990
Thalamus	252 ± 21	1000 ± 78	0.0207 ± 0.0032	449 ± 45	0.247 ± 0.067	296 ± 28	5.29 ± 1.46	0.991

TABLE 2
Coefficients of stress relaxation functions for various regions of the juvenile (P17/P18) rat brain (± 95% confidence intervals).

	G_∞ (Pa)	G_1 (Pa)	τ_1 (s)	G_2 (Pa)	τ_2 (s)	G_3 (Pa)	τ_3 (s)	G_4 (Pa)	τ_4 (s)	R^2
Alveus	245 ± 21	895 ± 102	0.0163 ± 0.0026	304 ± 35	0.34 ± 0.115	196 ± 32	5.25 ± 2.3			0.989
Brainstem	256 ± 9	874 ± 58	0.0176 ± 0.0022	303 ± 29	0.215 ± 0.055	243 ± 20	3.75 ± 0.66			0.990
Cerebellum Gray Matter	157 ± 32	529 ± 38	0.0262 ± 0.0037	229 ± 26	0.489 ± 0.15	185 ± 23	8.37 ± 4.17			0.988
Cerebellum White Matter	152 ± 13	1466 ± 391	0.0057 ± 0.0017	252 ± 22	0.202 ± 0.048	154 ± 18	4.87 ± 1.61			0.948
Corpus Callosum	148 ± 16	865 ± 99	0.0128 ± 0.002	289 ± 22	0.25 ± 0.057	253 ± 17	5.86 ± 1.27			0.984
Dentate Gyrus	220 ± 25	966 ± 103	0.0149 ± 0.0022	304 ± 27	0.305 ± 0.086	243 ± 23	6.53 ± 2.17			0.988
Hippocampus CA1	262 ± 29	5863 ± 7342	0.0013 ± 0.0024	406 ± 102	0.0366 ± 0.0186	309 ± 61	0.374 ± 0.153	226 ± 28	6.63 ± 2.87	0.982
Hippocampus CA3	280 ± 15	947 ± 78	0.017 ± 0.0022	400 ± 28	0.283 ± 0.061	277 ± 24	4.99 ± 1.14			0.996
Cortex	269 ± 14	920 ± 113	0.0145 ± 0.0029	366 ± 40	0.199 ± 0.057	276 ± 26	4.11 ± 0.93			0.989
Thalamus	230 ± 14	655 ± 40	0.0261 ± 0.0035	260 ± 31	0.316 ± 0.103	218 ± 23	4.97 ± 1.35			0.988

IV. DISCUSSION

The rat brain is viscoelastic, its viscoelastic properties evolve as the animal ages, and its mechanical properties vary across different anatomical structures. Our results agree with the findings of previous studies of the rat brain in orthogonal planes [17, 18]. Traumatic brain injury events occur at rapid rates so the viscoelasticity of the tissue must be quantitatively described in finite element models of these events to produce accurate predictions of brain deformation and injury risk. Young children and elderly adults are over-represented among patients suffering traumatic brain injuries [24]. It may be possible to better understand the reasons for this trend by including the age dependence of these tissues in finite element studies. Since juvenile rat brain tissue is softer than adult tissue, particularly at short time scales, it is reasonable to conclude that juvenile subjects undergo greater levels of tissue strain during an impact event. Larger strains may lead to more severe injury as compared to adult subjects [5, 6]. Finally, given that stiffness is unevenly distributed across anatomical structures within the brain, it is reasonable to assume that strain is also unevenly distributed across these structures during impact. Since strain drives axonal injury [25], the distribution of strain will combine with the distribution of strain tolerance to determine the distribution of injury. Quantitative description of these variations in finite element models will ultimately combine with local tolerance criteria and information about the function of each structure to yield deeper insight into the complex pathology of TBI. This insight is urgently needed because the heterogeneity of brain injury pathology is a significant barrier to progress in understanding its treatment [26].

The forebrain regions tested were stiffer than the cerebellum in both juvenile and adult animals. In adults, the stiffness of the brain stem was similar to that of the cerebellum while in juvenile animals, it was closer to that of the forebrain. The ANOVA revealed a significant interaction between the effect of age and time. This interaction was evident in the fact that the general trend towards stiffer properties as the tissue matures did not affect all regions and time points equally. The G_{10ms} values trended upward with maturation for all regions except the brain stem. The G_{50ms} values trended downwards with maturation for the brain stem and cerebellar white matter while the cerebellar grey matter was essentially unchanged, and the other regions tested trended upwards. The G_{20s} values trended downwards with maturation for the brain stem, alveus, cerebellar grey matter and thalamus while the other regions tested trended upwards. These results show that trends observed in static properties do not extend trivially to dynamic conditions and illustrate the importance of analyzing impact events using properties derived from experiments at relevant rates of loading. As in the preceding sagittal study, the G_{20s} values are on the same order as values reported previously for static moduli of rat brain tissue under indentation. AFM indentation of rat cerebellum yielded values similar to those presented here [27]. Microindentation of exposed rat brain *in vivo* yielded values somewhat higher than those reported here (508 Pa versus 328 Pa) [12], possibly because the indentation depths used were greater, and brain has been shown to strain harden under large compression [28].

The similarities and differences between this data set and the data set obtained during a previous analogous study in the sagittal plane [18] shed light on the dependence of mechanical properties on loading direction. Currently, the mathematical model employed to extract constitutive properties from experimental results is limited by the assumption of isotropy. A more sophisticated model will be needed to deduce anisotropic properties. Nevertheless, given the similarities between the two studies, it is reasonable to conclude that different properties obtained using the same test on the same structure in different planes imply that the structure in question is anisotropic. The adult G_{10ms} of the hind brain regions were similar in both planes, implying that these structures are isotropic. The alveus and corpus callosum were approximately 20% softer when tested in the horizontal plane as compared to the sagittal plane. There was also a significant decrease in the stiffness of the cortex and thalamus in the horizontal plane as compared to the sagittal plane while the properties recorded for the hippocampus in the horizontal plane were about half of what was measured in the sagittal plane. The juvenile data showed a similar pattern of isotropy in the hind brain and more anisotropy in the forebrain regions but the difference in the hippocampus was not as large as it was in the adult.

While these dramatic changes in the properties of certain regions with loading direction are intriguing, it is important to note the possibility that properties may vary with location within some larger anatomical structures. The anatomy and geometry of the brain are such that it is impossible to create horizontal and sagittal slices that intersect all regions at identical points in space. Specifically, the horizontal and sagittal experiments were performed at similar locations for small structures such as the hind brain regions, the alveus and the corpus callosum. However, larger, more peripheral structures such as the hippocampus and the cortex were tested at different locations in the two different planes. The sagittal plane intersected these structures close to the dorsal surface of the brain while the coronal plane intersected them several millimeters closer to the ventral surface of the brain. Therefore, the large differences between the horizontal and sagittal measurements of the properties of the hippocampus and cortex may reflect location-dependence as well as anisotropy in these structures. More focused experiments employing orthogonal cutting planes that intersect at a single point within one or other of these structures would be necessary to separate the effects of direction and location. By contrast, there is little possibility of a location-dependent effect explaining the difference between sagittal and horizontal measurements of the properties of the alveus and the corpus callosum so these differences were most likely solely due to anisotropy of these structures. This anisotropy may be due to the fact that these tissues primarily consist of aligned, myelinated, white matter fibers. The corpus callosum in particular consists of white matter fibers aligned with the left-right direction so the results suggest that compressing the tissue along the fiber direction generates more reaction force than compressing it across the fiber direction. Unfortunately, local fiber architecture varies widely across the brain so determining the local fiber direction at any point is not trivial. However, diffusion tensor imaging provides information about local fiber architecture at high spatial resolution [29], and ultimately it may be possible to estimate the principal directions of the stiffness matrix from these data sets.

As noted above, the current model is limited by the assumption of small strains and linear material properties implicit in the mathematical analysis employed. The approximation due to the assumption of small strains can be quantified by examining the definition of, for example, axial strain in the z direction at large strain (equation 5)

$$E_{zz} = \frac{1}{2}\left(\frac{du}{dz} + \frac{du}{dz} + \left(\frac{du}{dz}\right)^2\right) \quad (5)$$

where E is Lagrangian strain, u is motion in the z direction and z is the z co-ordinate. The small strain definition of the same strain differs only in that it lacks the second order term. In our experiment, the equivalent homogeneous axial strain is 10%. This implies that the neglected second order term is on the order of 0.5%.A recent review of the literature concludes that the linear viscoelastic limit of brain tissue was no more than 1% strain [30]. The strain field during indentation is heterogeneous with large tensile strains around the edge of the indenter, large compressive strains under the center of the indenter and small shear strains over a large region remote from the indenter. However, comparison of the system to an equivalent system undergoing homogeneous strain allows us to compute an equivalent compressive strain of 10% for this experiment. Injury to brain tissue typically requires strains of 10% or more [6] so experiments confined to the linear viscoelastic range would have little relevance to traumatic brain injury. Nevertheless, the linear viscoelastic model presented must be considered an approximation that provides a simple, robust description of the tissue relevant to more moderate traumatic brain injury scenarios. Since most investigators report that the non-linearity of brain tissue manifests as strain hardening [30], it is likely that the presented linear model overestimates stresses in the low strain regime remote from the indenter and underestimates stresses in the high strain regime close to the indenter. These limitations could be eliminated by replacing the current closed form mathematical model with an inverse finite element modeling approach. A non-linear finite element model would allow a more quantitative assessment of the approximation represented by a closed form linear model because it would allow measurement of the portion of the strain energy in the system that exists in regions remote from the indenter undergoing strain below the linear viscoelastic limit as compared to regions close to the indenter undergoing strains above this limit. The finite element method would also have the advantage of allowing incorporation of anisotropic material properties, moving the current qualitative discussion of material anisotropy on to a quantitative footing. It is likely that accurate representation of the anisotropy of brain tissue

(which has been reported by several investigators [13, 31]) would result in a redistribution of strain at any point in tissue from the direction of greatest stiffness to the direction of lowest stiffness. This redistribution could be particularly significant if the direction of material anisotropy follows the direction of axon alignment within the tissue because axons are vulnerable to stretch [32, 33]. Another challenge is the possibility that properties may vary not only between structures but also within structures, particularly large structures such as the hippocampus and cortex. It is possible to determine the small strain mechanical properties of the brain with high spatial resolution using magnetic resonance elastography (MRE) [34]. In light of this, another advantage of an inverse FEM treatment incorporating large strains would be that it might reveal a consistent relationship between large and small strain mechanical properties that could be used to extrapolate large strain properties at high spatial resolution from existing MRE data sets.

V. CONCLUSIONS

The data presented here demonstrate that mechanical properties of the rat brain depend on age, time domain, anatomy and, in the case of some regions, loading direction in the small strain domain. It is possible that spatial location also has an effect, independent of the effect of anatomy, and it remains to be seen if these trends will persist in the large strain domain. These data will allow us to formulate more detailed models of TBI that can begin to address questions of how various TBI events differ and what initiates the diverse pathophysiological processes that follow TBI.

VI. ACKNOWLEDGEMENT

The authors wish to thank Dr. Ed X. Guo for laboratory space and equipment. This study was supported by NHTSA Project # DTNH22-08-C-00088.

VII. REFERENCES

1. www.cdc.gov. [cited 2012 January 21]; Available from: http://www.cdc.gov/traumaticbraininjury/severe.html.
2. McAllister, T W, Neurobiological consequences of traumatic brain injury. *Dialogues Clin Neurosci*, 13 (3) p. 287-300, 2011.
3. Morganti-Kossmann, M C, E Yan, and N Bye, Animal models of traumatic brain injury: is there an optimal model to reproduce human brain injury in the laboratory? *Injury*, 41 Suppl 1 p. S10-3, 2010.
4. Mao, H, X Jin, L Zhang, K H Yang, T Igarashi, L J Noble-Haeusslein, et al., Finite element analysis of controlled cortical impact-induced cell loss. *J Neurotrauma*, 27 (5) p. 877-88, 2010.
5. Morrison, B, 3rd, H L Cater, C C Wang, F C Thomas, C T Hung, G A Ateshian, et al., A tissue level tolerance criterion for living brain developed with an in vitro model of traumatic mechanical loading. *Stapp Car Crash J*, 47 p. 93-105, 2003.
6. Cater, H L, L E Sundstrom, and B Morrison, 3rd, Temporal development of hippocampal cell death is dependent on tissue strain but not strain rate. *J Biomech*, 39 (15) p. 2810-8, 2006.
7. Galford, J E and J H McElhaney, A viscoelastic study of scalp, brain, and dura. *J Biomech*, 3 (2) p. 211-21, 1970.
8. Thibault, K L and S S Margulies, Age-dependent material properties of the porcine cerebrum: effect on pediatric inertial head injury criteria. *J Biomech*, 31 (12) p. 1119-26, 1998.
9. Bilston, L E, Z Liu, and N Phan-Thien, Linear viscoelastic properties of bovine brain tissue in shear. *Biorheology*, 34 (6) p. 377-85, 1997.
10. Miller, K and K Chinzei, Mechanical properties of brain tissue in tension. *J Biomech*, 35 (4) p. 483-90, 2002.
11. Chatelin, S, J Vappou, S Roth, J S Raul, and R Willinger, Towards child versus adult brain mechanical properties. *J Mech Behav Biomed Mater*, 6 p. 166-73, 2012.
12. Gefen, A, N Gefen, Q Zhu, R Raghupathi, and S S Margulies, Age-dependent changes in material properties of the brain and braincase of the rat. *J Neurotrauma*, 20 (11) p. 1163-77, 2003.
13. Prange, M T and S S Margulies, Regional, directional, and age-dependent properties of the brain undergoing large deformation. *J Biomech Eng*, 124 (2) p. 244-52, 2002.
14. Chatelin, S, A Constantinesco, and R Willinger, Fifty years of brain tissue mechanical testing: From in vitro to in vivo investigations. *Biorheology*, 47 (5) p. 255-76, 2010.
15. Garo, A, M Hrapko, J A van Dommelen, and G W Peters, Towards a reliable characterisation of the mechanical behaviour of brain tissue: The effects of post-mortem time and sample preparation. *Biorheology*, 44 (1) p. 51-8, 2007.
16. van Dommelen, J A, T P van der Sande, M Hrapko, and G W Peters, Mechanical properties of brain tissue by indentation: interregional variation. *J Mech Behav Biomed Mater*, 3 (2) p. 158-66, 2010.
17. Elkin, B S, A Ilankovan, and B Morrison Iii, A detailed viscoelastic characterization of the rat brain. *J Neurotrauma*, 2011.

18. Finan, J D, B S Elkin, E M Pearson, I L Kalbian, and B Morrison, 3rd, Viscoelastic properties of the rat brain in the sagittal plane: effects of anatomical structure and age. *Ann Biomed Eng*, 40 (1) p. 70-8, 2012.
19. Sneddon, I N, The Relation Between Load and Penetration in the Axisymmetric Boussinesq Problem for a Punch of Arbitrary Profile. *International Journal of Engineering Science*, 3 p. 47-57, 1965.
20. Hayes, W C, G Herrmann, L F Mockros, and L M Keer, A Mathematical Analysis for Indentation Tests of Articular Cartilage. *Journal of Biomechanics*, 5 (5) p. 541-&, 1972.
21. Lee, E H, Radok, J. R. M., The Contact Problem for Visooelastic Bodies. *Journal of Applied Mechanics*, 27 (3) p. 438-444, 1960.
22. Allen, M P, *Understanding Regression Analysis*. 1997, New York: Plenum Press.
23. Massey, F J, The Kolmogorov-Smirnov Test for Goodness of Fit. *Journal of the American Statistical Association*, 46 (253) p. 68-78, 1951.
24. Faul M, X L, Wald MM, Coronado VG., *Traumatic brain injury in the United States: emergency department visits, hospitalizations, and deaths.* 2010, Centers for Disease Control and Prevention, National Center for Injury Prevention and Control: Atlanta (GA).
25. LaPlaca, M C, D K Cullen, J J McLoughlin, and R S Cargill, 2nd, High rate shear strain of three-dimensional neural cell cultures: a new in vitro traumatic brain injury model. *J Biomech*, 38 (5) p. 1093-105, 2005.
26. Saatman, K E, A C Duhaime, R Bullock, A I Maas, A Valadka, and G T Manley, Classification of traumatic brain injury for targeted therapies. *J Neurotrauma*, 25 (7) p. 719-38, 2008.
27. Christ, A F, K Franze, H Gautier, P Moshayedi, J Fawcett, R J Franklin, et al., Mechanical difference between white and gray matter in the rat cerebellum measured by scanning force microscopy. *J Biomech*, 43 (15) p. 2986-92, 2010.
28. Miller, K and K Chinzei, Constitutive modelling of brain tissue: experiment and theory. *J Biomech*, 30 (11-12) p. 1115-21, 1997.
29. Veraart, J, T B Leergaard, B T Antonsen, W Van Hecke, I Blockx, B Jeurissen, et al., Population-averaged diffusion tensor imaging atlas of the Sprague Dawley rat brain. *Neuroimage*, 58 (4) p. 975-83, 2011.
30. Cheng, S, E C Clarke, and L E Bilston, Rheological properties of the tissues of the central nervous system: a review. *Med Eng Phys*, 30 (10) p. 1318-37, 2008.
31. Prange, M T, D F Meaney, and S S Margulies, Defining brain mechanical properties: effects of region, direction, and species. *Stapp Car Crash J*, 44 p. 205-13, 2000.
32. Bain, A C and D F Meaney, Tissue-level thresholds for axonal damage in an experimental model of central nervous system white matter injury. *J Biomech Eng*, 122 (6) p. 615-22, 2000.
33. Cloots, R J, J A van Dommelen, and M G Geers, A tissue-level anisotropic criterion for brain injury based on microstructural axonal deformation. *J Mech Behav Biomed Mater*, 5 (1) p. 41-52, 2012.
34. Clayton, E H, J R Garbow, and P V Bayly, Frequency-dependent viscoelastic parameters of mouse brain tissue estimated by MR elastography. *Phys Med Biol*, 56 (8) p. 2391-406, 2011.